

Type-II nodal loops: Theory and material realization

Si Li,^{1,2} Zhi-Ming Yu,² Ying Liu,² Shan Guan,^{1,2} Shan-Shan Wang,² Xiaoming Zhang,² Yugui Yao,^{1,*}
and Shengyuan A. Yang^{2,†}

¹Beijing Key Laboratory of Nanophotonics and Ultrafine Optoelectronic Systems, School of Physics, Beijing Institute of Technology, Beijing 100081, China

²Research Laboratory for Quantum Materials, Singapore University of Technology and Design, Singapore 487372, Singapore

(Received 4 May 2017; published 14 August 2017)

A nodal loop appears when two bands, typically one electronlike and one holelike, are crossing each other linearly along a one-dimensional manifold in reciprocal space. Here, we propose a type of nodal loop which emerges from the crossing between two bands which are both electronlike (or holelike) along a certain direction. Close to any point on such a loop (dubbed as a type-II nodal loop), the linear spectrum is strongly tilted and tipped over along one transverse direction, leading to marked differences in magnetic, optical, and transport responses compared with conventional (type-I) nodal loops. We show that the compound K_4P_3 is an example that hosts a pair of type-II nodal loops close to the Fermi level. Each loop traverses the whole Brillouin zone, and hence can only be annihilated in a pair when symmetry is preserved. The symmetry and topological protections of the loops as well as the associated surface states are discussed.

DOI: 10.1103/PhysRevB.96.081106

Topological metals and semimetals have become a focus of current physics research [1,2]. These materials feature nontrivial band crossings in their low-energy band structures, around which the quasiparticles behave drastically differently from the usual Schrödinger-type fermions. Depending on its dimensionality, the crossing manifold may take a zero-dimensional (nodal point), one-dimensional (nodal loop), or two-dimensional (nodal surface) form [3]. There have already been extensive studies on nodal points, especially on so-called Weyl and Dirac semimetal materials [4–17]. Recently, nodal loops have begun to attract considerable interest: Several nodal-loop materials have been proposed, with interesting physical consequences revealed [18–33].

Consider the generic case of a nodal loop formed by the linear crossing between two bands in a three-dimensional system. Close to any point P on the loop, the dispersion is linear along the two transverse directions of the loop, and is at least quadratic along the tangential direction. The low-energy effective model near P can be expressed as (set $\hbar = 1$)

$$\mathcal{H} = v_1 q_1 \sigma_x + v_2 q_2 \sigma_y + \mathbf{w} \cdot \mathbf{q}, \quad (1)$$

up to first order in the wave vector \mathbf{q} measured from P . Here, q_i 's ($i = 1, 2$) are the components of \mathbf{q} along two orthogonal transverse directions [see Fig. 1(a)], v_i 's are the Fermi velocities, and σ 's are Pauli matrices denoting the two-band degree of freedom. The last term with a vector \mathbf{w} in (1) represents a tilt of the spectrum, such that the energies of the two eigenstates $|u_{\pm}(\mathbf{q})\rangle$ are given by

$$E_{\pm} = \mathbf{w} \cdot \mathbf{q} \pm \sqrt{v_1^2 q_1^2 + v_2^2 q_2^2}. \quad (2)$$

In the q_1 - q_2 plane, the tilt is most effective along the \mathbf{w}_{\perp} direction, where $\mathbf{w}_{\perp} = (w_1, w_2, 0)$ is the projection of \mathbf{w} onto the q_1 - q_2 plane.

When $|\mathbf{w}_{\perp}|$ is small, the spectrum shows a usual band-crossing pattern for conventional nodal loops [see Fig. 1(b)]:

The crossing is of linear type, and the slopes of two bands have opposite signs for *all* directions in the q_1 - q_2 plane. The spectrum is then fully gapped along a small loop ℓ encircling the nodal loop [Fig. 1(a)], such that ℓ is characterized by a π Berry phase, $\oint_{\ell} \langle u_- | i \nabla_{\mathbf{q}} u_- \rangle \cdot d\mathbf{q} = \pi$, which may be intuitively understood by tracing the winding of the pseudospin σ for the lower band when moving around ℓ . When the system possesses both time reversal (\mathcal{T}) and inversion (\mathcal{P}) symmetries, and when the spin-orbit coupling (SOC) can be neglected, the Berry phase along any closed loop must be quantized in units of π [34], providing a topological protection of the nodal loop from a gap opening. Another commonly encountered protection mechanism comes from mirror reflection symmetry: A nodal loop in a mirror-invariant plane is protected when the two crossing bands have opposite mirror eigenvalues.

In this Rapid Communication, we propose the existence of a previously unrecognized type of nodal loop, which appears when $|\mathbf{w}_{\perp}|$ becomes large enough such that the tilt term dominates the spectrum in Eq. (2). This happens when $|\mathbf{w}_{\perp}|^2 > \sqrt{v_1^2 w_1^2 + v_2^2 w_2^2}$. In such a case, the spectrum becomes completely tipped over along the \mathbf{w}_{\perp} direction [Fig. 1(c)], where the two crossing bands now have the *same* sign for their slopes. (Note that for directions away from \mathbf{w}_{\perp} , the spectrum may still be of the usual type.) Parallel to the discussion in the context of nodal points [35,36], we term such types of loops as type II, to distinguish them from the conventional (type-I) nodal loops.

We first point out that type-II nodal loops could share the same protection mechanisms as their type-I counterparts. The Berry phase is still well defined, although there may not be a *global* gap along the loop ℓ (a local gap at each point on ℓ is sufficient for a well-defined Berry phase). Indeed, the winding of the pseudospin σ is not affected by the tilt, which only acts as a \mathbf{q} -dependent overall energy shift.

Consider the case when the loop lies in a mirror plane. Then the tilt vector \mathbf{w} is constrained to be in this plane. Assuming that \mathbf{w} is along the q_1 direction, the condition for a type-II (type-I) nodal loop becomes $|\mathbf{w}| > |v_1|$ ($|\mathbf{w}| < |v_1|$). One simplest

*ygyao@bit.edu.cn

†shengyuan_yang@sutd.edu.sg

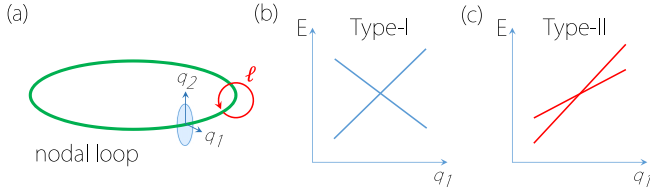


FIG. 1. (a) Schematic figure of a nodal loop. q_1 and q_2 label the two transverse directions. (b) and (c) illustrate the type-I and type-II dispersions along the q_1 direction.

model that describes a single nodal loop may be written as

$$H = \frac{1}{2m} k_\rho^2 + \frac{1}{2\eta} (k_\rho^2 - k_0^2) \sigma_x + v_z k_z \sigma_y, \quad (3)$$

where $k_\rho = \sqrt{k_x^2 + k_y^2}$, m , η , and k_0 are model parameters. The model describes a nodal loop with radius k_0 in the $k_z = 0$ plane. Evidently, it contains (1) as a low-energy model via identifying q_1 to be along the in-plane radial direction \hat{k}_ρ , and q_2 to be along \hat{k}_z direction, with the correspondences that $v_1 = k_0/\eta$, and $\mathbf{w} = k_0/m\hat{k}_\rho$. Hence the loop is type II (type I) when $|\eta/m| > 1$ (< 1). One observes that in the type-I case, the loop is formed by the crossing between an electronlike band and a holelike band, whereas for $|\eta/m| > 1$, the tilt term [first term in Eq. (3)] dominates, making both bands electronlike or holelike along the radial direction depending on the sign of m , and their intersection makes a type-II nodal loop.

The distinction between type-II and type-I loops can be observed from the geometry of their constant energy surfaces, which are shown in Figs. 2(a) and 2(b) for the q_1 - q_2 plane

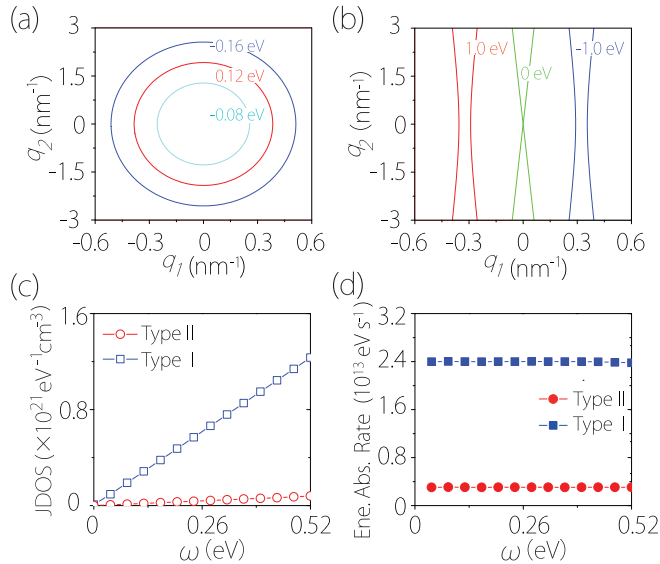


FIG. 2. Equienergy contours in the q_1 - q_2 plane for (a) type-I and (b) type-II loops. Comparison of (c) JDOS and (d) optical energy absorption rate for the two types of loops. Here, we used model (3) with parameters $k_0 = 1.7 \text{ nm}^{-1}$, $\eta = 0.4m_e$ (m_e is the free electron mass), and $v_z = 1 \times 10^5 \text{ m/s}$. We take $m = 0.04m_e$ for the type-II case and $m \rightarrow \infty$ for the type-I case. The Fermi level is set at the loop's energy for each case. In (d), the light E field is polarized along the y direction with a peak value of 0.1 mV/nm .

(k_ρ - k_z plane) intersecting the ring. One observes that for a type-I loop, the equienergy contours are closed ellipses encircling the loop. When the Fermi energy is aligned to that of the loop (set as zero energy in the figure), the Fermi surface is simply given by the loop. In contrast, the equienergy contours for a type-II loop become hyperbolas [37], and at the energy of the loop, the contour coincides with the two asymptotes.

The qualitative difference between the shapes of their constant energy surfaces will manifest in a variety of physical properties. For example, under a magnetic field, electrons orbit around constant energy surfaces, the different types of orbits will produce contrasting signals in magneto-oscillations [38–40] (such as de Haas–van Alphen oscillations), and the transition from elliptic- to hyperbolic-type orbits, e.g., by varying the magnetic field direction for a type-II nodal loop, would typically be accompanied by a Landau level collapse phenomenon [41].

One notes from Figs. 2(a) and 2(b) that the positive and negative energy contours have a much smaller overlap for a type-II loop than for a type-I loop. This is a natural consequence of both bands being electronlike (or holelike), and could lead to a marked difference in their optical response. Assuming the Fermi level is at the loop's energy, the optical absorption involves transitions from negative energy states to positive energy states at the *same* k point. Compared to the type-I case, the positive and negative energy states for a type-II loop are largely separated in k space, leading to much smaller absorption at low energies. This difference can be inferred from the joint density of states (JDOS), $\mathcal{D}(\omega) = \frac{1}{V} \sum_k \delta(E_{c,k} - E_{v,k} - \omega)$, and the optical energy absorption rate, $\mathcal{R}(\omega) = 2\pi\omega \sum_k |M_{cv}|^2 \delta(E_{c,k} - E_{v,k} - \omega)$. Here, M_{cv} is the optical transition matrix element, and note that E_c (E_v) is for states above (below) the Fermi level. In Figs. 2(c) and 2(d), we plot JDOS and \mathcal{R} (for light with linear polarization in the xy plane) calculated for the model in Eq. (3). One indeed observes that both quantities are much suppressed for the type-II case.

We also briefly remark that for carrier transport in the plane of the loop, the type-II loop may have a higher mobility than the type-I case. This is because that while they both share an enhancement due to the π Berry phase [20], the low-energy states near a point on the type-II loop are propagating roughly at the same direction, while the opposite-propagating states are located at the other end of the loop (cf. Fig. 1), thus momentum relaxation by scattering would be less efficient as compared with the type-I case [42].

We now describe a concrete material realization for the type-II nodal loops—the crystalline compound K_4P_3 . The single-crystal K_4P_3 solid has been synthesized experimentally through a reaction of red phosphorous with excess potassium [43]. The material is a stable paramagnetic metal at ambient condition, taking a W_3CoB_3 -type orthorhombic structure with space group No. 63 ($Cmcm$) [43] [see Fig. 3(a)]. The structure has angular P_3 chains, with each P atom lying in the center of a trigonal prism formed by six K^+ ions [44,45]. Detailed structure information can be found in Ref. [43], and experimental lattice parameters ($a = b = 6.141 \text{ \AA}$, $c = 14.788 \text{ \AA}$) [43] are used in the calculation. For the following discussion, it is important to note the presence of two symmetries: the

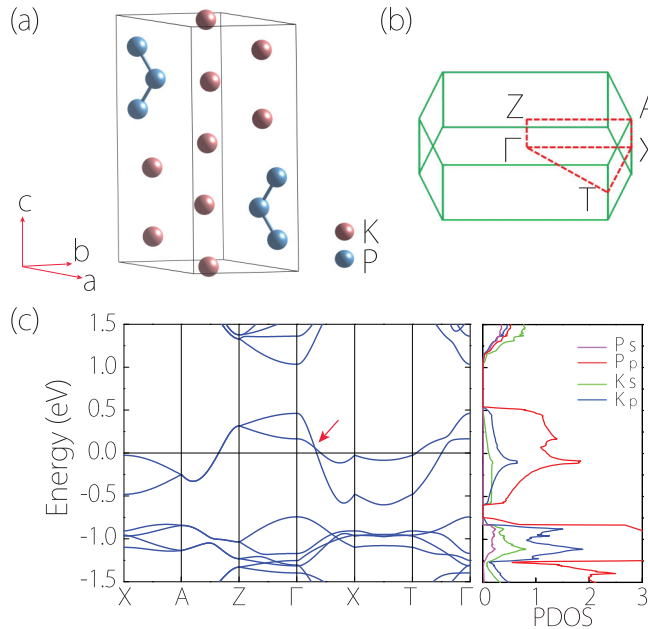


FIG. 3. (a) Crystal structure of K_4P_3 . (b) Brillouin zone with high symmetry points labeled. (c) Electronic band structure of K_4P_3 and the projected density of states (PDOS). The red arrow indicates the crossing point on a type-II nodal loop.

inversion symmetry \mathcal{P} and the glide mirror symmetry \mathcal{M} about the (110) plane [with $(x, y, z) \rightarrow (x, -y, z + 1/2)$].

We performed first-principles calculations based on the density functional theory (DFT), as implemented in the Vienna *ab initio* simulation package [46,47]. The ionic potentials were modeled with the projector augmented wave method [48], and the exchange-correlation functional was approximated in the generalized gradient approximation with the Perdew-Burke-Ernzerhof (PBE) realization [49]. The cutoff energy was chosen as 400 eV, and the Brillouin zone (BZ) was sampled with a Γ -centered k mesh of size $12 \times 12 \times 6$. The energy and force convergence criteria were set to be 10^{-5} eV and 0.01 eV/Å, respectively. The band structures with and without SOC show very little difference, hence SOC is neglected in the following discussion. The surface states were investigated using the method with maximally localized Wannier functions [50–52].

The band structure of K_4P_3 is shown in Fig. 3(c). One observes that the system is metallic, and from the projected density of states (PDOS), the low-energy states are mainly from the p orbitals of P atoms. There are two low-energy bands, which cross each other linearly along Γ -X, forming a crossing point as indicated in Fig. 3(c). Since the system preserves both \mathcal{P} and \mathcal{T} symmetries, which dictates a vanishing Berry curvature field [53], this linear crossing point cannot be isolated. Indeed, a careful scan of the band structure reveals that the crossing between the two bands forms a pair of nodal loops, as illustrated in Figs. 4(a) and 4(b). The two loops are lying in the (110) plane, as constrained by the \mathcal{M} symmetry, and they are quite straight. The energy variation along the loops is small (<0.01 eV), and the loops can be brought even closer to the Fermi level by doping or applying pressure [54].

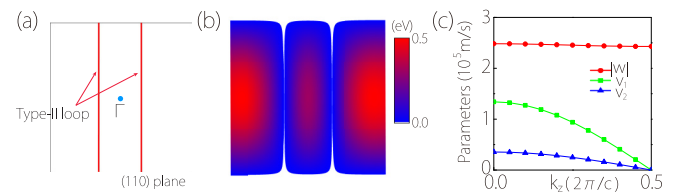


FIG. 4. (a) Schematic figure showing the location of the type-II loops in the (110) plane, and (b) shows the corresponding result from DFT. The color map shows the local gap between the two crossing bands. (c) Parameters of effective model (1) obtained by fitting the DFT band structure.

Interestingly, each loop traverses the whole BZ, a feature that has important consequences to be discussed below.

Most important for our discussion is the observation that the dispersion around the loop is of type II in the mirror plane along the $[\bar{1}10]$ direction. Model (1) can be used to fit the DFT band structure. Since each loop is almost a straight line along k_z , q_1 and q_2 can be taken as orthogonal components along the $[\bar{1}10]$ and $[110]$ directions, respectively. The tilt vector w is in the q_1 direction as required by \mathcal{M} , and its sign is opposite for the two loops. The fitted parameters are plotted in Fig. 4(c). The value of $|w|$ slightly varies around 2.5×10^5 m/s, while both v_1 and v_2 are maximum at $k_z = 0$ and approach zero towards the Brillouin zone boundary. Most importantly, one observes that $|w| > |v_1|$ for the whole loop, therefore, the loop is type II.

The type-II loops here have two independent symmetry protections. One protection is from the \mathcal{P} and \mathcal{T} symmetries, which ensures a quantized π Berry phase for any close path encircling each loop. The other protection is from \mathcal{M} since the two crossing bands have opposite \mathcal{M} eigenvalues, as we have checked in the DFT result. Consequently, the loop is stable against perturbations as long as one of the two protections is preserved.

Here, each type-II loop is traversing the whole BZ. Such a kind of loop is topologically distinct from those which are not penetrating the BZ, because the former cannot be continuously contracted to a point [3], whereas the latter can. Mathematically, the BZ is topologically equivalent to a three-dimensional torus \mathbb{T}^3 . Closed loops on \mathbb{T}^3 can be classified under its fundamental homotopy group $\pi_1(\mathbb{T}^3) = \mathbb{Z}^3$, labeled by three integers, each indicating the number of times the loop winds around one of the three directions. In this sense, the nodal loops not traversing BZ belong to the trivial class with $\mathbb{Z}^3 = (0,0,0)$ (which includes a single point), whereas the loops here belong to the $(0,0,1)$ class. Hence the two kinds

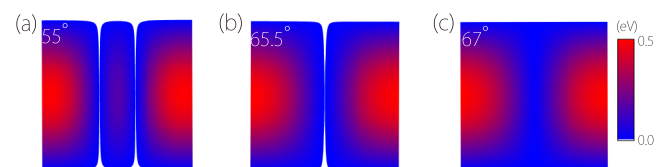


FIG. 5. Evolution of the loops when changing the angle γ between the a and b axis, for (a) $\gamma = 55^\circ$, (b) $\gamma = 65.5^\circ$, and (c) $\gamma = 67^\circ$.

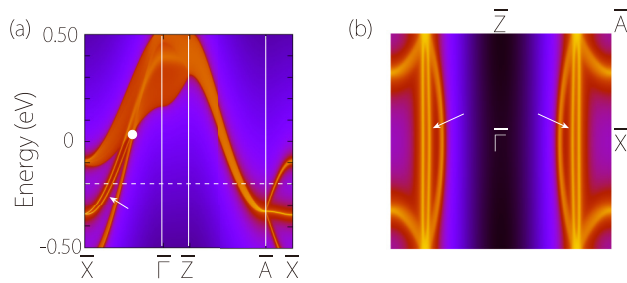


FIG. 6. (a) Projected spectrum on the (110) surface, and (b) the corresponding constant energy slice at -0.2 eV. The white dot in (a) marks the projected bulk band-crossing point. The arrows indicate the drumheadlike surface states.

of loops cannot be continuously deformed into each other. This also means that with preserved symmetry, each of the two loops here cannot be annihilated by itself; they can only annihilate in a pair. One such scenario is shown in Fig. 5, where we vary the angle γ between the a and b axis, which preserves the crystal symmetry. With increasing γ , the two loops are moving towards the BZ center and finally annihilate with each other.

Nodal loops usually possess drumheadlike surface states [18]. In Fig. 6, we show the spectrum of the (110) surface of K_4P_3 . Indeed, one observes the drumhead surface band emanated from the bulk nodal points. The surface band connects the two loops through the surface BZ boundary. We verify that each bulk line along the [110] direction and in the surface band region carries a quantized π Berry phase, hence

contributing a state at the surface terminated by vacuum [54]. One also notes an additional surface band with slightly higher energy which we find is originated from the surface dangling bonds.

Before closing, we mention that the type-II nodal loops in K_4P_3 and the associated surface states can be directly probed via angle-resolved photoemission spectroscopy. In addition, the type-II nature of the loops may also manifest in the contrast between DOS and JDOS, and in the magnetic response of K_4P_3 , as discussed in Ref. [54]. We also point out that besides type-I and type-II loops, there could also be a hybrid type for which the tilt vector dominates only over part of the loop. In terms of physical properties, the hybrid type should be intermediate between type I and type II. We find real materials that possess such hybrid loops, e.g., in the ScCd-type transition-metal intermetallic materials [55]. Hybrid nodal lines connecting nexus points have also been predicted in Bernal stacked graphite [56–58]. Finally, for K_4P_3 , the direction of the tilt vector is pinned onto the glide mirror plane, but for systems with reduced symmetry, the tilt vector may wind around when going along the loop. How such a variation would affect physical properties could be an interesting topic to investigate in future works.

The authors thank X.-L. Sheng, Y. X. Zhao, X. C. Wu, and D. L. Deng for valuable discussions. This work was supported by the MOST Project of China (No. 2014CB920903), the National Natural Science Foundation of China (Grant No. 11574029), and Singapore MOE AcRF Tier 1 (SUTD-T1-2015004) and Tier 2 (MOE2015-T2-2-144).

- [1] A. A. Burkov, *Nat. Mater.* **15**, 1145 (2016).
- [2] B. Yan and C. Felser, *Annu. Rev. Condens. Matter Phys.* **8**, 337 (2017).
- [3] S. A. Yang, *SPIN* **06**, 1640003 (2016).
- [4] X. Wan, A. M. Turner, A. Vishwanath, and S. Y. Savrasov, *Phys. Rev. B* **83**, 205101 (2011).
- [5] S. Murakami, *New J. Phys.* **9**, 356 (2007).
- [6] A. A. Burkov and L. Balents, *Phys. Rev. Lett.* **107**, 127205 (2011).
- [7] G. E. Volovik, *The Universe in a Helium Droplet* (Clarendon, Oxford, UK, 2003).
- [8] S. M. Young, S. Zaheer, J. C. Y. Teo, C. L. Kane, E. J. Mele, and A. M. Rappe, *Phys. Rev. Lett.* **108**, 140405 (2012).
- [9] Z. Wang, Y. Sun, X.-Q. Chen, C. Franchini, G. Xu, H. Weng, X. Dai, and Z. Fang, *Phys. Rev. B* **85**, 195320 (2012).
- [10] Y. X. Zhao and Z. D. Wang, *Phys. Rev. Lett.* **110**, 240404 (2013).
- [11] B.-J. Yang and N. Nagaosa, *Nat. Commun.* **5**, 4898 (2014).
- [12] H. Weng, C. Fang, Z. Fang, B. A. Bernevig, and X. Dai, *Phys. Rev. X* **5**, 011029 (2015).
- [13] S.-M. Huang, S.-Y. Xu, I. Belopolski, C.-C. Lee, G. Chang, B. Wang, N. Alidoust, G. Bian, M. Neupane, C. Zhang, S. Jia, A. Bansil, H. Lin, and M. Z. Hasan, *Nat. Commun.* **6**, 7373 (2015).
- [14] Z. K. Liu, B. Zhou, Y. Zhang, Z. J. Wang, H. M. Weng, D. Prabhakaran, S.-K. Mo, Z. X. Shen, Z. Fang, X. Dai, Z. Hussain, and Y. L. Chen, *Science* **343**, 864 (2014).
- [15] S. Borisenko, Q. Gibson, D. Evtushinsky, V. Zabolotnyy, B. Büchner, and R. J. Cava, *Phys. Rev. Lett.* **113**, 027603 (2014).
- [16] B. Q. Lv, H. M. Weng, B. B. Fu, X. P. Wang, H. Miao, J. Ma, P. Richard, X. C. Huang, L. X. Zhao, G. F. Chen, Z. Fang, X. Dai, T. Qian, and H. Ding, *Phys. Rev. X* **5**, 031013 (2015).
- [17] S.-Y. Xu, I. Belopolski, N. Alidoust, M. Neupane, G. Bian, C. Zhang, R. Sankar, G. Chang, Z. Yuan, C.-C. Lee, S.-M. Huang, H. Zheng, J. Ma, D. S. Sanchez, B. Wang, A. Bansil, F. Chou, P. P. Shibayev, H. Lin, S. Jia, and M. Z. Hasan, *Science* **349**, 613 (2015).
- [18] H. Weng, Y. Liang, Q. Xu, R. Yu, Z. Fang, X. Dai, and Y. Kawazoe, *Phys. Rev. B* **92**, 045108 (2015).
- [19] S. A. Yang, H. Pan, and F. Zhang, *Phys. Rev. Lett.* **113**, 046401 (2014).
- [20] K. Mullen, B. Uchoa, and D. T. Glatzhofer, *Phys. Rev. Lett.* **115**, 026403 (2015).
- [21] R. Yu, H. Weng, Z. Fang, X. Dai, and X. Hu, *Phys. Rev. Lett.* **115**, 036807 (2015).
- [22] Y. Kim, B. J. Wieder, C. L. Kane, and A. M. Rappe, *Phys. Rev. Lett.* **115**, 036806 (2015).
- [23] Y. Chen, Y. Xie, S. A. Yang, H. Pan, F. Zhang, M. L. Cohen, and S. Zhang, *Nano Lett.* **15**, 6974 (2015).
- [24] L. S. Xie, L. M. Schoop, E. M. Seibel, Q. D. Gibson, W. Xie, and R. J. Cava, *APL Mater.* **3**, 083602 (2015).
- [25] C. Fang, Y. Chen, H.-Y. Kee, and L. Fu, *Phys. Rev. B* **92**, 081201 (2015).

- [26] Y.-H. Chan, C.-K. Chiu, M. Y. Chou, and A. P. Schnyder, *Phys. Rev. B* **93**, 205132 (2016).
- [27] R. Li, H. Ma, X. Cheng, S. Wang, D. Li, Z. Zhang, Y. Li, and X.-Q. Chen, *Phys. Rev. Lett.* **117**, 096401 (2016).
- [28] G. Bian, T.-R. Chang, R. Sankar, S.-Y. Xu, H. Zheng, T. Neupert, C.-K. Chiu, S.-M. Huang, G. Chang, I. Belopolski, D. S. Sanchez, M. Neupane, N. Alidoust, C. Liu, B. Wang, C.-C. Lee, H.-T. Jeng, C. Zhang, Z. Yuan, S. Jia, A. Bansil, F. Chou, H. Lin, and M. Z. Hasan, *Nat. Commun.* **7**, 10556 (2016).
- [29] L. M. Schoop, M. N. Ali, C. Straer, A. Topp, A. Varykhalov, D. Marchenko, V. Duppel, S. S. P. Parkin, B. V. Lotsch, and C. R. Ast, *Nat. Commun.* **7**, 11696 (2016).
- [30] C. Fang, H. Weng, X. Dai, and Z. Fang, *Chin. Phys. B* **25**, 117106 (2016).
- [31] Y. Jin, R. Wang, J. Zhao, C. Zheng, L.-Y. Gan, J. Liu, H. Xu, and S. Y. Tong, [arXiv:1608.05791](https://arxiv.org/abs/1608.05791).
- [32] L.-Y. Gan, R. Wang, Y. J. Jin, D. B. Ling, J. Z. Zhao, W. P. Xu, J. F. Liu, and H. Xu, *Phys. Chem. Chem. Phys.* **19**, 7245 (2017).
- [33] R. Yu, Q. Wu, Z. Fang, and H. Weng, *Phys. Rev. Lett.* **119**, 036401 (2017).
- [34] A. P. Schnyder, S. Ryu, A. Furusaki, and A. W. W. Ludwig, *Phys. Rev. B* **78**, 195125 (2008).
- [35] A. A. Soluyanov, D. Gresch, Z. Wang, Q. Wu, M. Troyer, X. Dai, and B. A. Bernevig, *Nature (London)* **527**, 495 (2015).
- [36] Y. Xu, F. Zhang, and C. Zhang, *Phys. Rev. Lett.* **115**, 265304 (2015).
- [37] The open contour in the effective model can become closed when the model is regularized on a lattice.
- [38] T. E. O'Brien, M. Diez, and C. W. J. Beenakker, *Phys. Rev. Lett.* **116**, 236401 (2016).
- [39] F.-Y. Li, X. Luo, X. Dai, Y. Yu, F. Zhang, and G. Chen, *Phys. Rev. B* **94**, 121105 (2016).
- [40] S. Khim, K. Koepernik, D. V. Efremov, J. Klotz, T. Förster, J. Wosnitza, M. I. Sturza, S. Wurmehl, C. Hess, J. van den Brink, and B. Büchner, *Phys. Rev. B* **94**, 165145 (2016).
- [41] Z.-M. Yu, Y. Yao, and S. A. Yang, *Phys. Rev. Lett.* **117**, 077202 (2016).
- [42] S. Guan, Z.-M. Yu, Y. Liu, G.-B. Liu, L. Dong, Y. Lu, Y. Yao, and S. A. Yang, *npj Quantum Mater.* **2**, 23 (2017).
- [43] H. G. von Schnering, M. Hartweg, U. Hartweg, and W. Hönle, *Angew. Chem., Int. Ed. Engl.* **28**, 56 (1989).
- [44] J. M. Sangster, *J. Phase Equilib. Diffus.* **31**, 68 (2010).
- [45] R. Pöttgen, W. Hönle, and H. G. von Schnering, in *Encyclopedia of Inorganic and Bioinorganic Chemistry* (Wiley, Hoboken, NJ, 2011).
- [46] G. Kresse and J. Hafner, *Phys. Rev. B* **49**, 14251 (1994).
- [47] G. Kresse and J. Furthmüller, *Phys. Rev. B* **54**, 11169 (1996).
- [48] P. E. Blöchl, *Phys. Rev. B* **50**, 17953 (1994).
- [49] J. P. Perdew, K. Burke, and M. Ernzerhof, *Phys. Rev. Lett.* **77**, 3865 (1996).
- [50] N. Marzari and D. Vanderbilt, *Phys. Rev. B* **56**, 12847 (1997).
- [51] I. Souza, N. Marzari, and D. Vanderbilt, *Phys. Rev. B* **65**, 035109 (2001).
- [52] Q. S. Wu, S. N. Zhang, H.-F. Song, M. Troyer, and A. A. Soluyanov, [arXiv:1703.07789](https://arxiv.org/abs/1703.07789).
- [53] D. Xiao, M.-C. Chang, and Q. Niu, *Rev. Mod. Phys.* **82**, 1959 (2010).
- [54] See Supplemental Material at <http://link.aps.org/supplemental/10.1103/PhysRevB.96.081106> for Berry phase calculation, experimental signatures of type-II loops, and K_4P_3 under pressure or time reversal symmetry breaking.
- [55] S. Li *et al.* (unpublished).
- [56] T. T. Heikkilä and G. E. Volovik, *New J. Phys.* **17**, 093019 (2015).
- [57] T. Hyart and T. T. Heikkilä, *Phys. Rev. B* **93**, 235147 (2016).
- [58] K. Zhang and G. E. Volovik, [arXiv:1604.00849](https://arxiv.org/abs/1604.00849).